D7

DEVELOPMENT OF HEAT FLUX SENSORS FOR TURBINE AIRFOILS AND COMBUSTOR LINERS

William H. Atkinson
Pratt & Whitney Aircraft Group
Engineering Division

This paper briefly describes the work performed under two contracts: NAS3-23529, "Turbine Blade and Vane Heat Flux Sensor Development"; and a pre-HOST effort, NAS3-22133, "Advanced High Temperature Heat Flux Sensor Development". The objective of each of these contracts is to develop heat flux sensors for use on gas turbine engine hot section components.

The design of durable turbine airfoils that use a minimum amount of cooling air requires knowledge of the heat loads on the airfoils during engine operation. Measurement of these heat loads will permit the verification or modification of the analytical models used in the design process and will improve the ability to predict and confirm the thermal performance of turbine airfoil designs. Heat flux sensors for turbine blades and vanes must be compatible with the cast nickel-base and cobalt-base materials used in their fabrication and will need to operate in a hostile environment with regard to temperature, pressure and thermal cycling. There is also a need to miniaturize the sensors to obtain measurements without perturbing the heat flows that are to be measured.

At the start of the turbine blade and vane program, a literature search and a survey of commercially available sensors were conducted to determine the current state of the art for heat flux sensors. These investigations revealed that there were no existing sensors which met the geometrical and environmental requirements of the blade and vane heat flux measurements. An effort was then initiated to develop feasible sensor designs for turbine blade and vane applications. Several concepts were chosen for further consideration:

- o embedded thermocouple sensors using the airfoil wall as a thermal barrier,
- o Gardon gage sensors fabricated into the airfoil wall,
- o several types of transient sensors.

Sensor concepts that were only suitable for transient testing were subsequently dropped from consideration because of the complexity of introducing sufficiently rapid transient conditions into the hot side heat transfer coefficient or into the airfoil coolant during actual engine testing.

Figure 1 is a schematic of the embedded thermocouple sensor. This type of one dimensional steady state sensor determines the heat flux by measuring the temperature drop across a thermal barrier. In this case, the airfoil wall itself acts as the thermal barrier. The Gardon gage sensor is shown schematically in figure 2. This type of steady state sensor determines the heat flux from the temperature rise due to radial conduction from the insulated section of the hot side of the airfoil wall. Both these sensors have been optimized for steady state conditions but may also be used as transient heat flux sensors.

A series of thermoelectric tests were conducted on blade and vane alloys to determine the suitability of these materials as thermoelectric elements. The use of the airfoil material in the thermoelectric circuit gives a direct differential output and reduces the number of wires required, minimizing the potential for temperature perturbations caused by the presence of the wires. All of the

superalloys tested were found to produce positive thermoelectric outputs with temperature when paired with platinum. These thermoelectric outputs were stable throughout four thermal cycles and several hours of thermal soaking. Alumel was selected as the preferred thermoelectric material because of the relatively high voltage output, availability and low cost. Millivolt outputs versus temperature of the various superalloys when paired with Alumel are presented in figure 3.

The sensor designs were analyzed for thermal performance using a three dimensional finite difference heat transfer program (TCAL) developed at Pratt & Whitney Aircraft. This program determined the thermal perturbations caused by the presence of the sensor and the theoretical outputs to be expected from the sensor. This information was used to calculate the anticipated error in the heat flux indicated by the sensor compared with the heat flux that existed in the unperturbed airfoil.

Both the embedded thermocouple and Gardon gage sensor designs were fabricated into first stage turbine blade halves. For the embedded thermocouple sensors, grooves were eloxed into the inner and outer airfoil surfaces. The thermocouples were installed in the grooves using a wedge wire technique, and the surface of the installation was smoothed off. Figures 4 and 5 show the interior and exterior walls of a typical installation. The blade halves were then welded together and the assembled blade is shown in figure 6.

For the Gardon gage sensors, a cavity was eloxed into the interior wall of the blade half and a groove was eloxed to route the leadwire away from the sensor. To minimize the number of grooves required, the Gardon gage sensor used a three wire swaged lead. The thermocouple junctions were made in the cavity by resistance welding, and the leadwire was installed in the groove using a wedge wire technique. The cavity was then filled with a ceramic cement to provide oxidation and mechanical protection for the thermocouple wires and to restore the aerodynamic integrity of the internal blade wall. Figure 7 shows the completed Gardon gage sensor on the interior blade surface.

A calibration fixture, shown in figure 8, was designed and fabricated for the calibration of airfoil-mounted heat flux sensors. This fixture is mounted below a quartz lamp bank heat source, shown in figure 9. The fixture allows positioning of the airfoil so that the surface of the heat flux sensor is normal to the incident radiation. The surface of the airfoil is coated with material having a known and stable absorptance and emittance. The incident radiation is measured with a reference Hy-Cal asymptotic calorimeter. This same test apparatus is used for thermal cycle tests and thermal soak tests as well as the calibration tests.

Data from the calibration of a typical embedded thermocouple sensor are shown in figures 10 and 11. Figure 11 shows that sensor sensitivity (sensor output/heat flux transmitted) varies with temperature. This would be expected because of variation in the thermal conductivity of the blade material and the thermoelectric output with temperature. If these factors are analytically accounted for, the sensor output can be normalized to an 1150 K sensor reference temperature. The normalized data for this sensor are presented in figures 12 and 13. Similarly, data for a typical Gardon gage sensor are presented in figures 14 and 15. These data normalized to an 1150 K sensor reference temperature are shown in figures 16 and 17.

Several sensors were subjected to thermal cycling tests, in which the sensors were rapidly heated to near maximum temperature and heat flux, held at this condition for one minute, cooled rapidly to near ambient temperature and held there

for three minutes. The normal test program was 50 thermal cycles. Calibration data for a typical sensor before and after the thermal cycle test are shown in figure 18. Thermal soak tests were also conducted on several sensors in which the sensor was held at near maximum temperature and heat flux for a period of 10 hours. Calibration data for a typical sensor before and after the thermal soak test are shown in figure 19.

The sensors developed under the first phase of the turbine blade and vane heat flux sensor program have been shown to be capable of measuring the heat loads on turbine airfoils with an accuracy of ±10 percent, and have withstood thermal cycling and thermal soak conditions that are to be expected to be representative of a gas turbine engine environment. A second phase of this program will demonstrate a wide variety of heat transfer measurement methods on a simple test piece in an atmospheric combustor rig. This work, just recently initiated, will consist of running a cylinder in cross flow behind a laboratory combustor rig. The first portion of this work will be to characterize the combustor exit as fully as possible with respect to temperature, pressure and velocity, including the spatial and temporal variations of these quantities. Various types of heat flux sensors and other heat flux measurement instrumentation will be mounted in cylindrical test sections and tested behind the combustor. This instrumentation will include both transient and steady state sensors as well as instrumentation for measuring dynamic gas and metal temperatures. The results of the various measurement techniques will be correlated and compared with the analytically predicted heat flux levels.

Under a pre-HOST NASA contract (Contract NAS3-22133, "Advanced High Temperature Heat Flux Sensor Development", from the NASA LeRC Instrumentation R&D Branch) described in Reference 1, high temperature steady state heat flux sensors were designed and fabricated for use in combustor liners. There were three sensor designs generated:

- o the laminated sensor,
- o the Gardon gage sensor,
- o the embedded thermocouple sensor.

Figure 20 shows a schematic representation of each of these sensors. The sensors were subjected to laboratory testing consisting of calibrations, thermal cycle tests and thermal soak tests. The test results on these sensors were presented at the 1982 HOST Contractor's Workshop.

In a continuation of that contractual effort, a combustor liner has been instrumented with eight heat flux sensors and is ready to be tested in a high pressure combustor facility. There are three Gardon gage sensors, three embedded thermocouple sensors and two laminated sensors mounted in the combustor liner. An overall view of the cold side of the liner is shown in figure 21, and a close up view of the cold side of two of the sensors is shown in figure 22. The hot side of one of the sensors, presented in figure 23, shows the resistance weld around the periphery of the sensor that was used to fasten the sensor into the liner wall. After the sensors were installed into the liner, a functional check was performed to verify that they were still operational. The liner will be run as a part of the test sequence on NASA Contract NAS3-22392, "Broad Specification Fuels Program".

These high pressure combustor tests will also include two radiometer probes for measuring the radiative portion of the total heat load. These two radiometers, a porous plug radiometer probe developed at Pratt & Whitney Aircraft and a commercially available Medtherm radiometer probe, are shown in figure 24. The porous

plug radiometer probe has a field of view nearly 180 degrees while the Medtherm radiometer has a 50 degree field of view. During the test, the two radiometers will be mounted on opposite walls facing each other as shown in figure 25. In this configuration, both probes will view the same volume and, hence, the signals should correlate. It is anticipated that the two probe locations will be interchanged during the test program to eliminate any rig bias. It is hoped that the data from these tests will help clarify some of the wide angle and narrow angle radiometer data taken in other test programs.

As a result of the two contracts for heat flux sensor development, high temperature steady state heat flux sensors have been fabricated for use on turbine blades and vanes and on combustor liners. The use of these sensors in upcoming test programs will provide detailed information on the heat loads on hot section components, and will represent a significant advance in the modeling and prediction of the heat transfer characteristics of gas turbine engines.

REFERENCE

1. Atkinson, W. H.: and Strange, R.R.: "Development of Advanced High-Temperature Heat Flux Sensors: NASA CR-165618: September 1982.

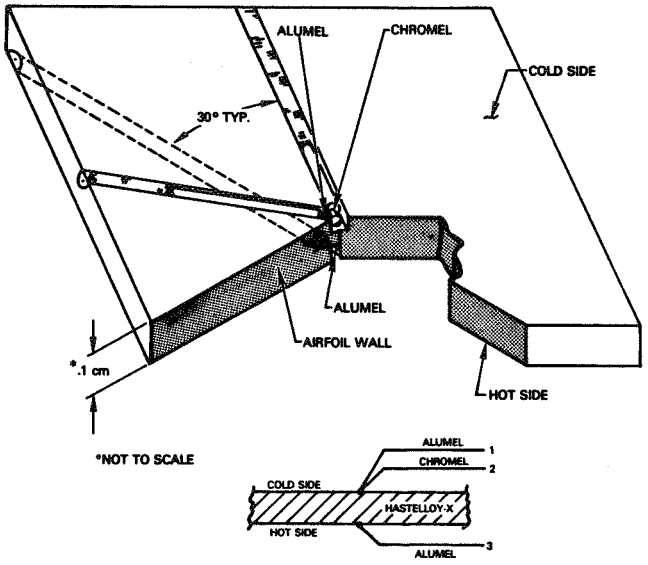

Figure 1 Schematic of Embedded Thermocouple Sensor

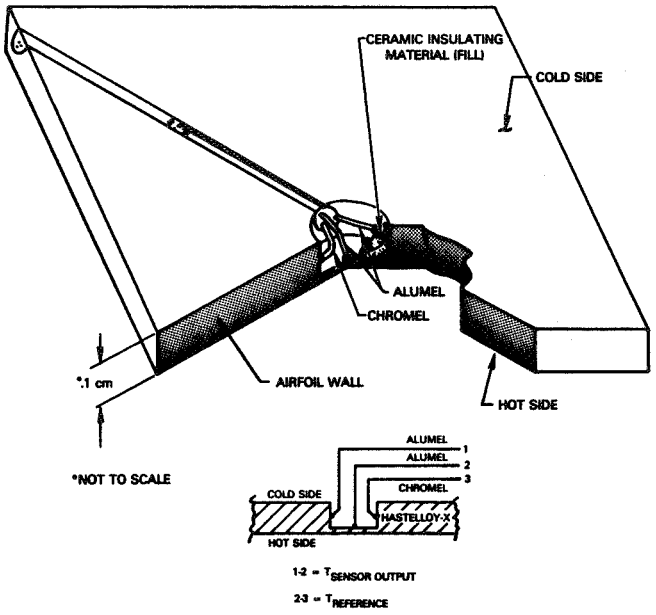

Figure 2 Schematic of Gardon Gage Sensor

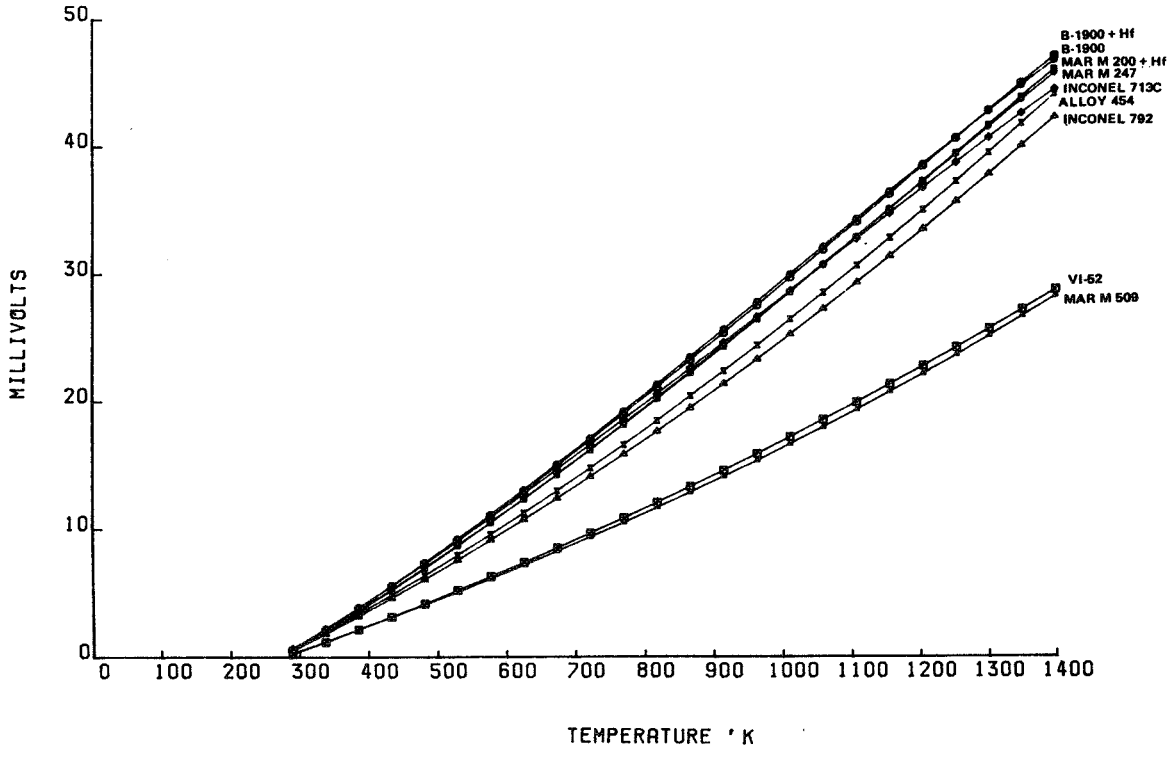

Figure 3 Plot of Thermoelectric Output of Superalloys versus Alumel

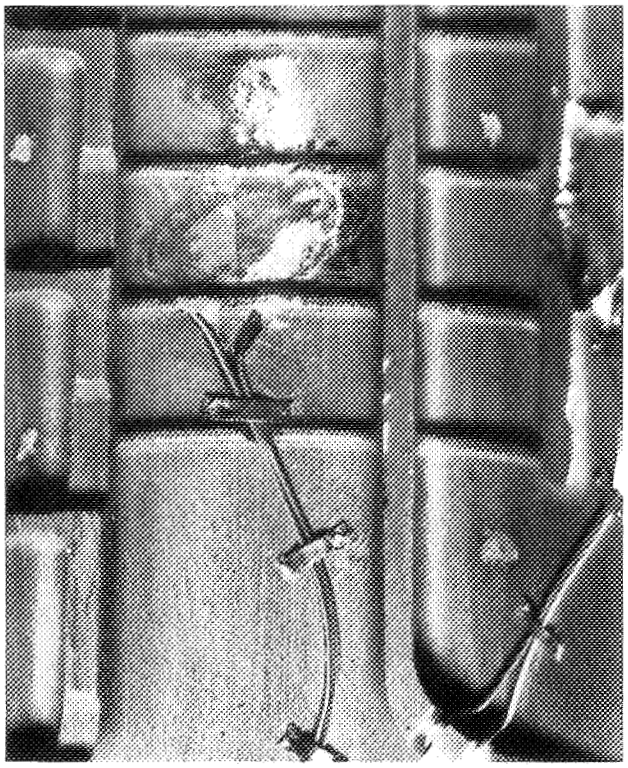

Figure 4 View of Interior Wall of Embedded Thermocouple Sensor

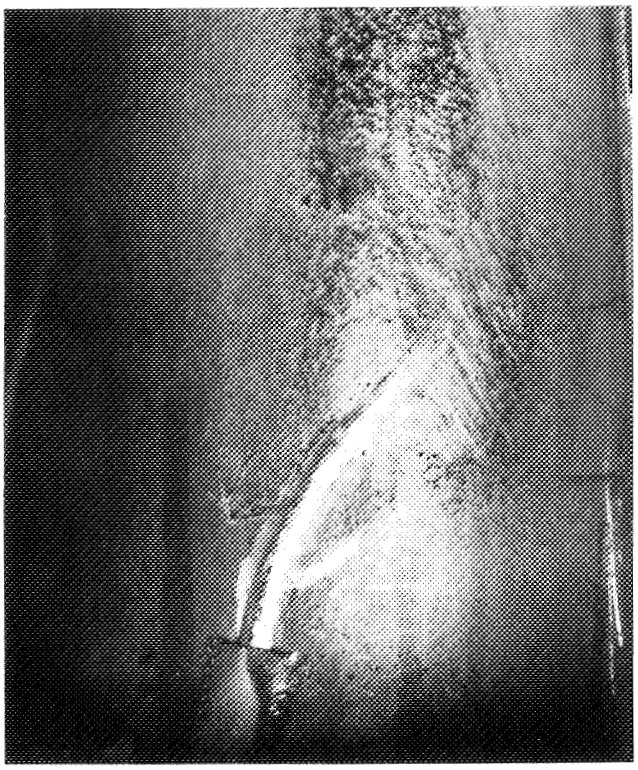

Figure 5 View of Exterior Wall of Embedded Thermocouple Sensor

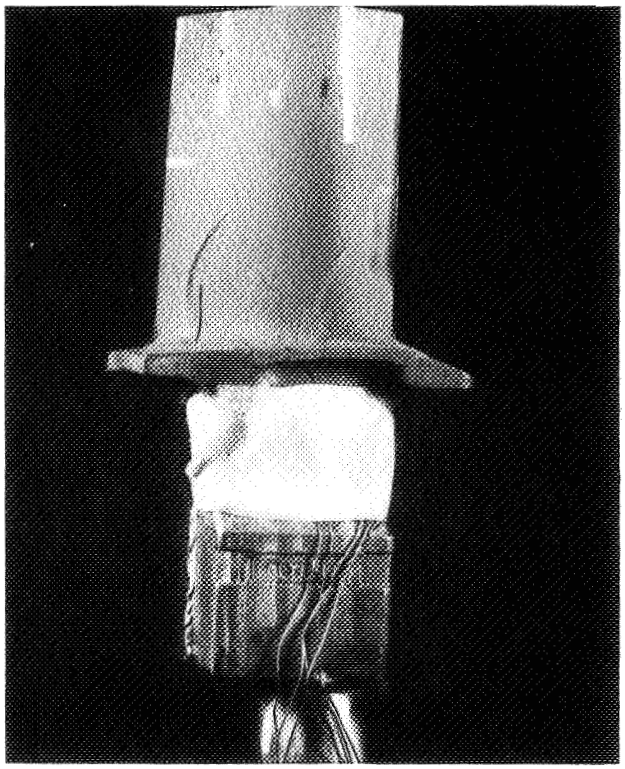

Figure 6 View of Assembled Embedded Thermocouple Instrumented Blade

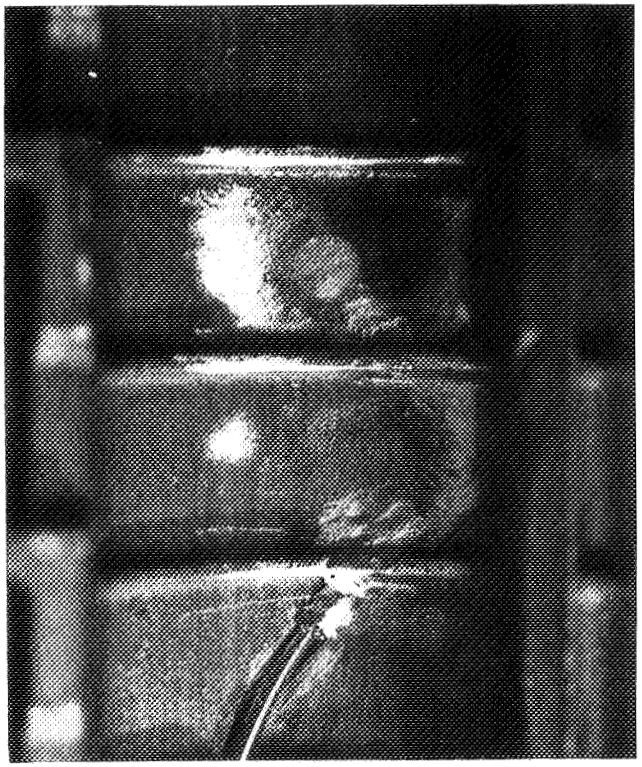

Figure 7 View of Interior Wall of Gardon Gage Sensor

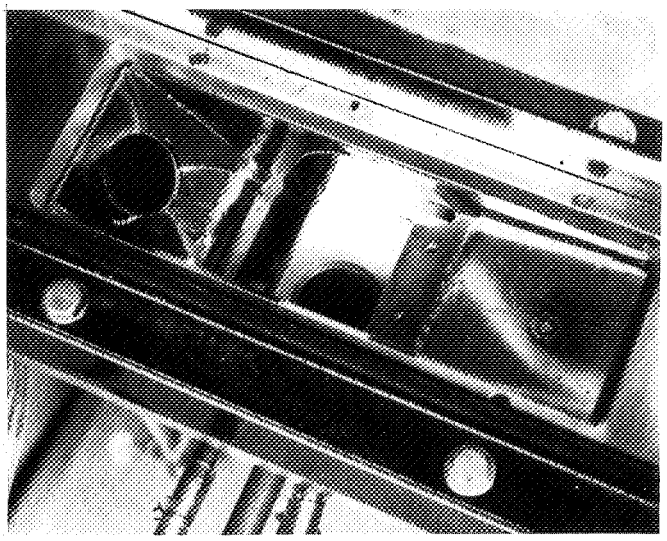

Figure 8 View of Calibration Fixture

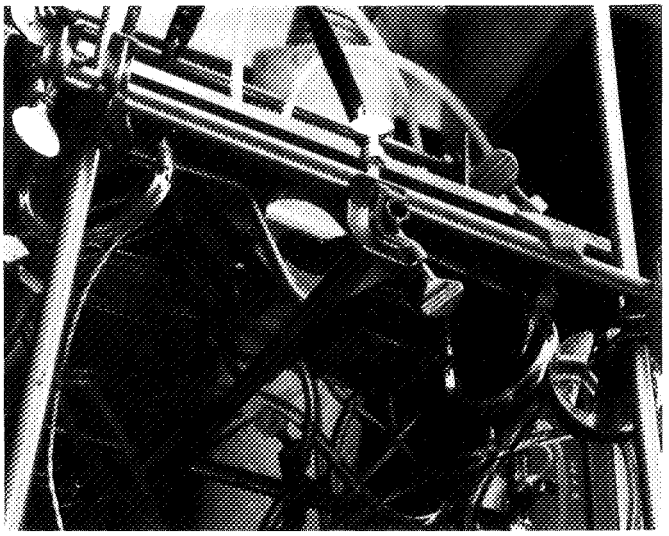

Figure 9 View of Calibration Setup

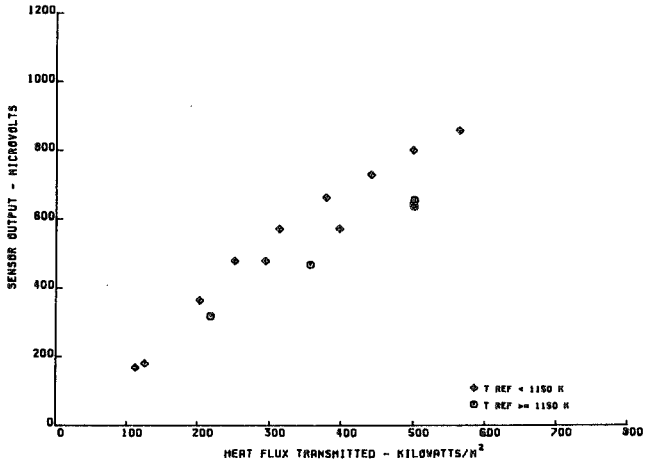

Figure 10 Plot of Output versus Heat Flux for Embedded Thermocouple Sensor

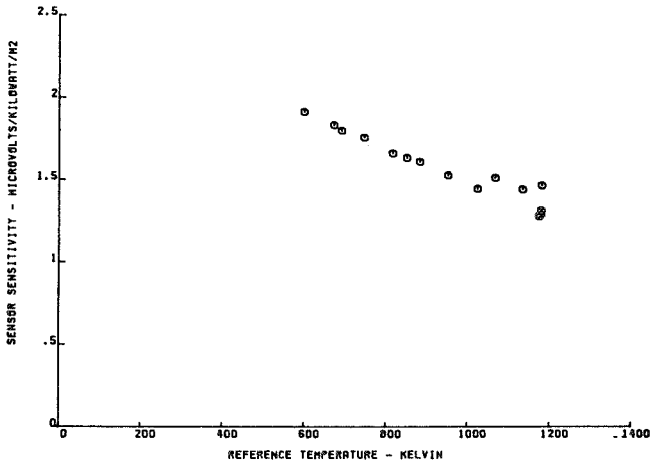

Figure 11 Plot of Sensitivity versus Temperature for Embedded Thermocouple Sensor

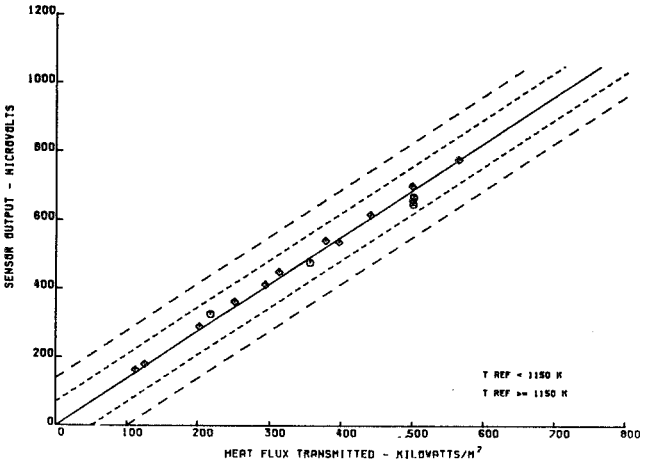

Figure 12 Plot of Normalized Output versus Heat Flux for Embedded Thermocouple Sensor

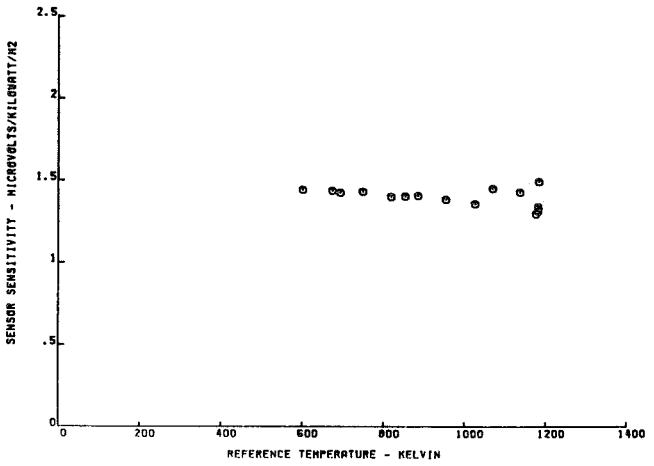

Figure 13 Plot of Normalized Sensitivity versus Temperature for Embedded Thermocouple Sensor

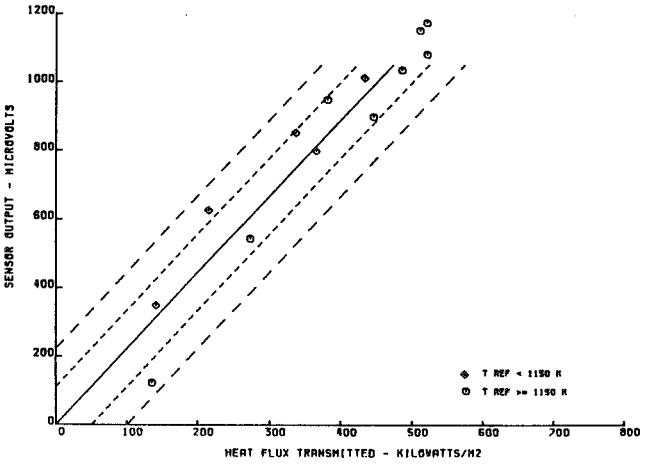

Figure 14 Plot of Output versus Heat Flux for Gardon Gage Sensor

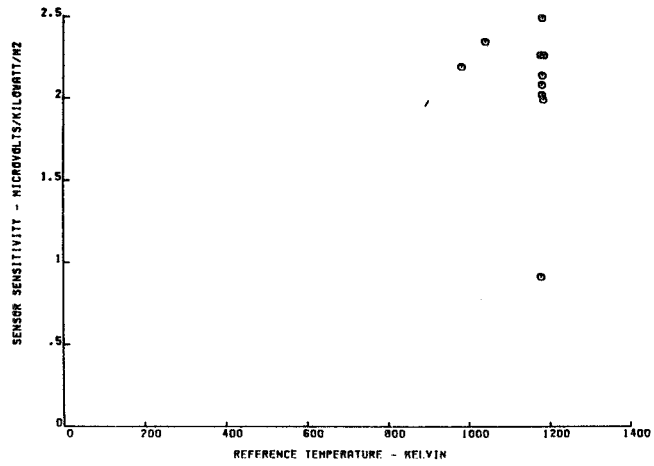

Figure 15 Plot of Sensitivity versus Temperature for Gardon Gage Sensor

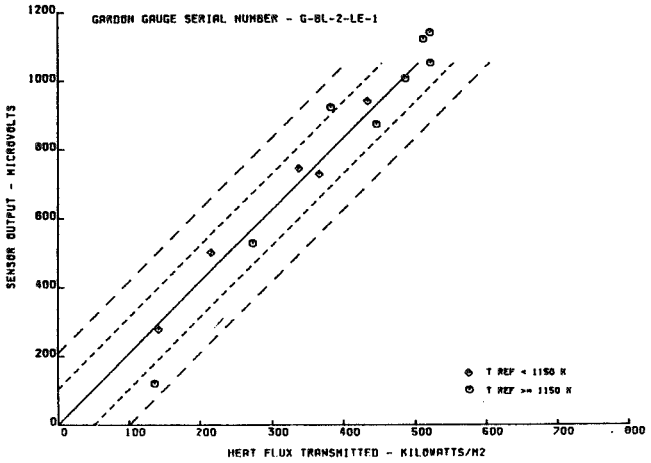

Figure 16 Plot of Normalized Output versus Heat Flux for Gardon Gage Sensor

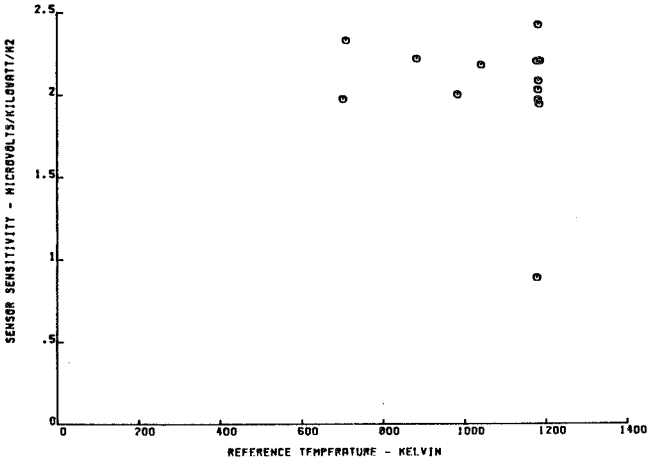

Figure 17 Plot of Normalized Sensitivity versus Temperature for Gardon Gage Sensor

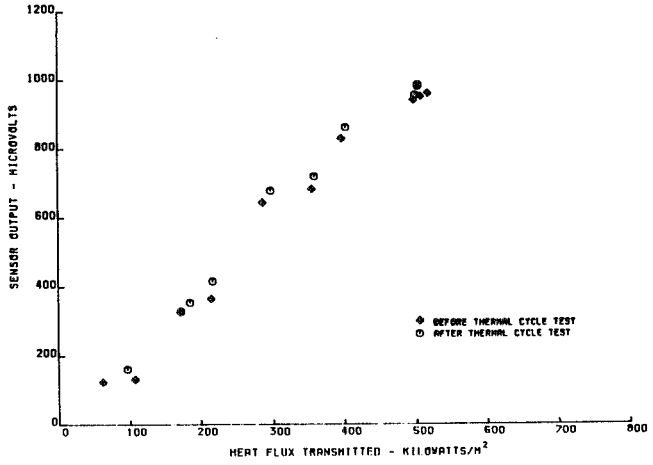

Figure 18 Plot of Data before and after Thermal Cycle Test

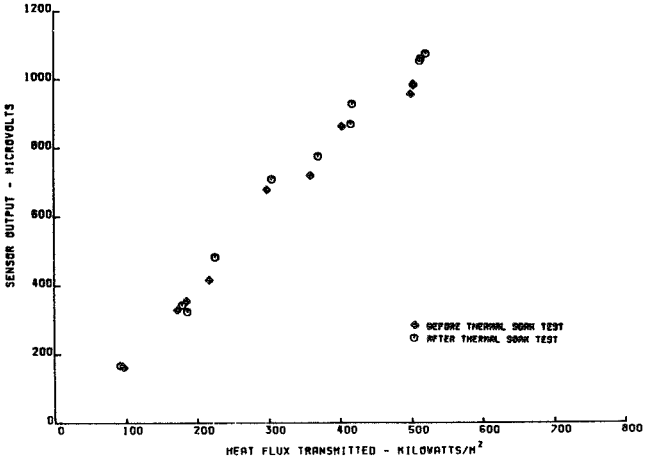

Figure 19 Plot of Data before and after Thermal Soak Test

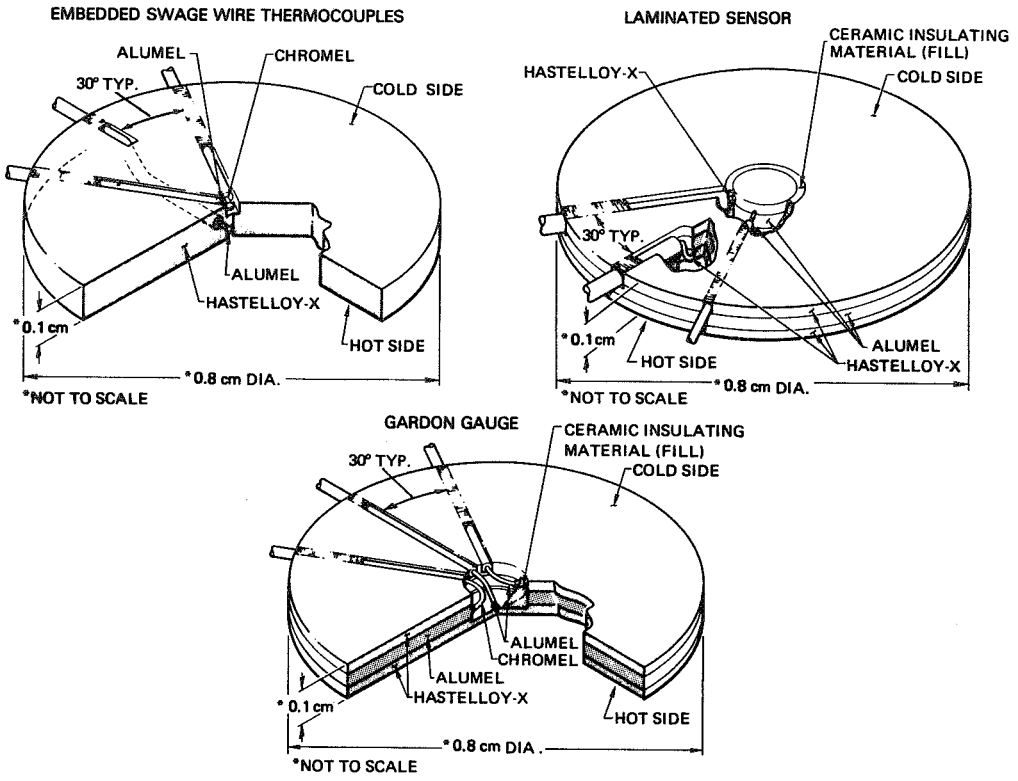

Figure 20 Schematic Representation of Combustor Liner Sensors

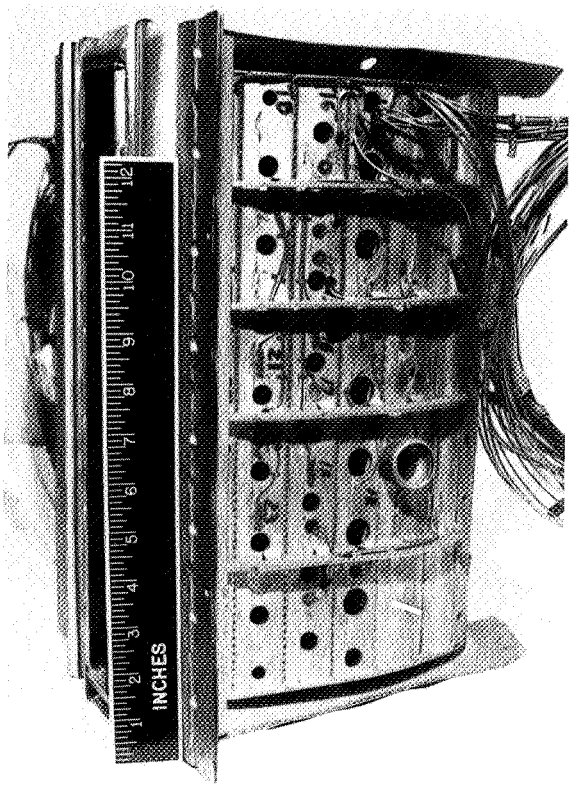

Figure 21 View of Cold Side of Instrumented Combustor Liner

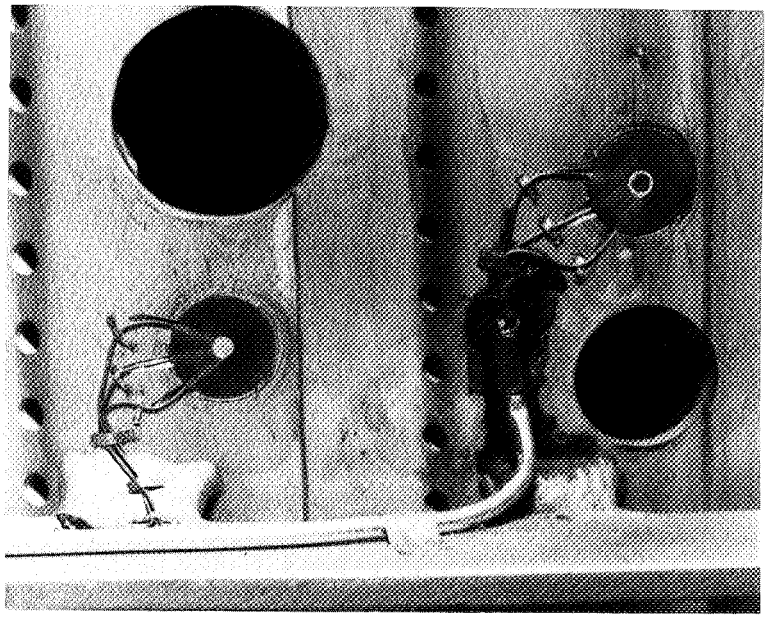

Figure 22 Close up View of Cold Side of Two Combustor Liner Heat Flux Sensors

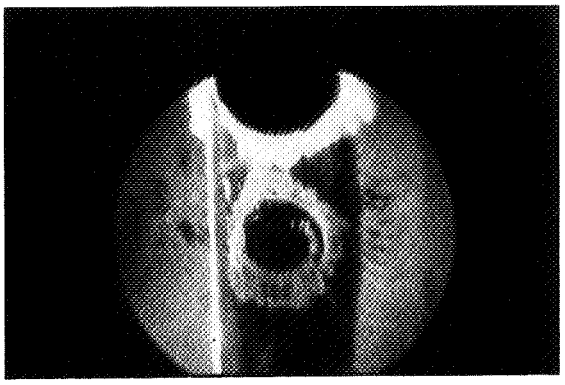

Figure 23 Close up View of Hot Side of Combustor Liner Heat Flux Sensor

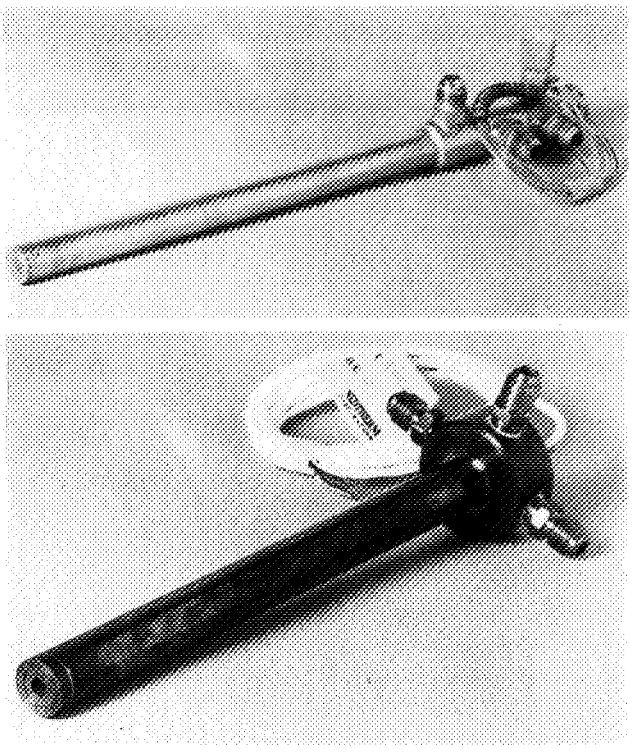

Figure 24 View of Porous Plug and Medtherm Radiometer Probes

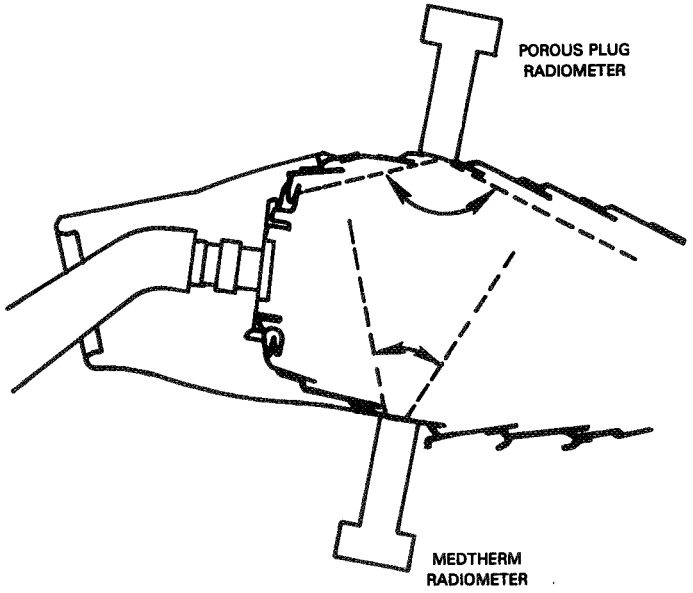

Figure 25 Schematic Representation of Radiometer Installation